IEEE Access
Multidisciplinary ⋮ Rapid Review ⋮ Open Access Journal

Received 21 March 2024, accepted 7 April 2024, date of publication 10 April 2024, date of current version 17 April 2024.

Digital Object Identifier 10.1109/ACCESS.2024.3387054

RESEARCH ARTICLE

Partitioned Ohtomo Stability Test for Efficient Analysis of Large-Signal Solutions

SERGIO COLANGELI[1], LEONARDO PANTOLI[2], (Member, IEEE), WALTER CICCOGNANI[1], PATRICK E. LONGHI[1], (Member, IEEE), GIORGIO LEUZZI[2], AND ERNESTO LIMITI[1], (Senior Member, IEEE)

[1]Department of Electronics Engineering, University of Rome Tor Vergata, 00133 Rome, Italy
[2]Department of Industrial and Information Engineering and Economy, University of L'Aquila, 67100 L'Aquila, Italy

Corresponding author: Sergio Colangeli (colangeli@ing.uniroma2.it)

ABSTRACT A fundamental step in the design of electronic circuits is the verification that they are stable at least on a given set of external terminations, in order to avoid that the solution found be not observable in practice. This is especially true at microwave and millimeter-wave circuits, which are typically analyzed in the frequency domain rather than in the time domain. As a consequence, both in the linear and large-signal case, unstable solutions may be found instead of an observable one. Unfortunately, as compared to the linear case, the stability analysis of large-signal solutions is significantly more cumbersome. In particular, although it is possible to translate the small-signal tests based on the Nyquist principle to large-signal equivalents, the price to pay is a significant increase in matrix size. In the case of the Ohtomo test, which has only recently been applied to large-signal solutions, it is however possible to exploit the structure of the problem to significantly reduce the complexity and, therefore, simulation time. A real-world balanced amplifier is selected to validate the proposed method and illustrate its practical usage. The application of the method to a realistic monolithic circuit with a large number of devices is also presented.

INDEX TERMS Harmonic balance, microwaves, nonlinear circuits, Ohtomo test, stability analysis.

I. INTRODUCTION

Electronic circuits operating at frequencies high enough that distributed effects cannot be neglected (most notably, in the microwave and millimeter-wave ranges) are typically analyzed in the frequency domain through the Harmonic Balance (HB) algorithm rather than in the time domain. As a consequence, the solutions returned by the circuit simulator are by construction periodic [1], [2]. Nevertheless, there is no *a priori* guarantee that the equilibria considered in the analysis will be stable: quite to the contrary, the possibility exists that the simulated solution is unstable and, as such, not observable in the fabricated circuits [3]. This represents a problem to the designers of high-frequency circuits, especially amplifiers (both in the small-signal and large-signal regimes) but also frequency multipliers and mixers. Conversely, being able to reliably detect the startup conditions of autonomous oscillations is also important in the design of oscillators and frequency dividers.

Although there exists a variety of easy-to-use tools to investigate the stability of d.c. solutions [4], [5] or even the unconditional stability of linear 2-ports [6], [7], the large-signal case is significantly harder to tackle. Since the latter can be reduced to a linear problem through linearization, the difficulty does not really arise so much from a theoretical difference as, rather, from an increase in the dimension of the problem. Thus, both in the linear and nonlinear case, the established theory of linear dynamical systems [8] can be exploited. Ultimately, the stability analysis reduces to studying the zeros of the characteristic polynomial associated with the solution at hand, with only a few exceptions [3], [9], [10], [11], [12].

In order to localize the zeros of the characteristic polynomial on the complex plane, two main approaches can be recognized in the literature: namely, identification-based techniques [13], [14], [15] and Nyquist-based techniques [1],

The associate editor coordinating the review of this manuscript and approving it for publication was Photos Vryonides.

[16], [17], [18], [19], [20]. Although the former are easier to implement and use, the latter are significantly more user-independent and reliable if they are fed the full description of the circuit under consideration, from the vantage point of a circuit section for which observability [8] can be assumed. This full description is obtained by computing, for each perturbation frequency of a reasonably extended sweep, the whole conversion matrices [2] of two P-port sub-circuits, where P is a potentially large number of ports. If the HB order is denoted by H, these matrices have size $N \times N$, with $N = (2H+1)P$: thus, the problem size increases quadratically with H and P.

In this contribution, a peculiarity of the Ohtomo test (a stability analysis tool first generalized to the large-signal regime in [20]) is exploited to overcome the 'curse of dimensionality' inherent in previous stability tests based on the combined usage of the Nyquist principle and conversion matrices. The results are expected to be of significant interest to designers of microwave integrated circuits (MICs) and monolithic MICs (MMICs) such as power amplifiers, frequency multipliers, mixers and, secondarily, oscillators and frequency dividers.

The implementation described in this work is based on Keysight's Advanced Design System (ADS [21]), but equivalent adaptations in other commercial Electronic Design Automation (EDA) environments, such as Cadence's Microwave Office [22], are clearly possible, by exploiting the relevant scripting capabilities. Notice that the simulation data are processed and the Nyquist plots produced directly within the EDA environment (rather than relying on external mathematical software, such as MATLAB [23]) by extensive use of custom functions in the Application Extension Language (AEL).

The manuscript is organized as follows. Section II will provide some background on the problem at hand. Section III will introduce the key idea, i.e., the partitioning of the Ohtomo test. Section IV will demonstrate that, thanks to the partitioning, the efficiency of the test improves significantly as compared to the standard approach (from quadratic to linear in the number of active devices). Section V will show that the proposed approach provides correct results when applied to a well known test vehicle, but with significantly improved efficiency than the standard approach. An example on how to use the proposed approach to verify the efficacy of stabilization techniques is also illustrated. Section VI will present the application of the presented approach to a realistic MMIC, with state-of-the-art performance and comprising a large number of active devices. For the Reader's convenience, a summary of the main symbols and acronyms is presented in Tables 1 and 2, respectively.

II. THEORETICAL BACKGROUND

The reader is referred to Ohtomo's original paper [4] for the general setup and the basic notation, with particular reference to the definition of the stability matrix $\mathbf{M}_N(s)$ and of the loop gains $\underline{G}_k(s)$. It is in that paper that the scattering representation is used for the first time in the stability analysis of linear circuits, with some advantages in the verification of the 'inherent stability' proviso, i.e., a theoretical precondition for the Nyquist principle to be applied safely. In practice, this and similar methods are typically applied to linearized d.c. solutions rather than to actually linear circuits.

Consider, on the other hand, the case of forced periodic solutions in nonlinear circuits (the most representative example being that of power amplifiers with continuous-wave inputs of nonnegligible level), as typically found through the HB algorithm. The stability of these solutions can be analyzed by injecting a small signal and considering the perturbed solution, which can be expressed as the superposition of the original orbit (i.e., periodic solution) and of its linearization. This is analogous to the linear case, except that the linearized portion of the solution is now represented by a conversion matrix [2].

As a consequence, the theoretical tools available to analyze the stability of large-signal solutions are basically the same as for the small-signal case, as mentioned in the Introduction. With specific reference to the Nyquist-based techniques, the two which most clearly appear as translations of small-signal approaches are presented in [18] and [20]. If we exclude the aspects pertaining to the implementation, these two approaches simply differ by the representation of choice, i.e., impedance or admittance in the former, scattering in the latter.

Thus, the theoretical validity of these methods is already well established. Nevertheless, the actual implementation becomes important in practice for reasons of computational efficiency, since the size of the conversion matrices involved in typical circuits grows quickly with the number of active devices, harmonic components and small-signal frequencies. The present contribution builds up on [20] and provides a partitioned formulation of the network determinant, which ultimately leads to a significantly improved implementation, as illustrated in Section III and quantified in Section IV.

As to the actual computation of the conversion matrices, this is performed, in the EDA environment of choice, through a large-signal/small-signal (LSSS) simulation [2]. To start, denote with $I^{p}_{f_{SS}}$ a perturbation current at port p and frequency f_{SS}, and with $V^{p'}_{f_{SS}+hf_{LS}}$ a response voltage at port p' and frequency $f_{SS}+hf_{LS}$, where $-H \le h \le +H$. Then:

$$Z^{p',p}_{f_{SS}+hf_{LS},f_{SS}} = \left.\frac{V^{p'}_{f_{SS}+hf_{LS}}}{I^{p}_{f_{SS}}}\right|_{oc} \tag{1}$$

where the 'oc' subscript specifies an open-circuit termination for all ports and small-signal frequencies. The orderly compilation (by p and h) of all such terms results in the conversion matrix of the considered network in the impedance representation. Admittance and scattering conversion matrices can be computed either directly through analogous procedures or, alternatively, by changing the representation (through textbook formulas) of an already available conversion matrix.

TABLE 1. Definition of main symbols used throughout the paper.

Symbol	Definition	Further reading
n, b, h, k, l	running indexes	
H	order of the HB algorithm	[1]
p_b	number of physical ports of block b	
n_b	number of (physical or virtual) ports of block b $n_b = (2H+1)\,p_b$	
B	number of blocks of the active sub-network	
P	number of physical ports of the passive and active sub-networks $P = p_b B$ (assuming uniform blocks)	
N	number of (physical or virtual) ports of the passive and active sub-networks $N = (2H+1)\,P$	
N_b	index of first (physical or virtual) port of block b, minus 1 $\sum_{l=1}^{b-1} n_l$	
F	number of small-signal frequencies	
f_{LS}	frequency of the large-signal excitation (driving signal)	
f_{SS}	frequency of the small-signal excitation (perturbation signal)	
s	complex (i.e., Laplace's) frequency	[8]
$\mathbf{1}$	identity matrix (of appropriate size)	
$\mathbf{S}(s)$	scattering matrix of the active sub-network	[4]
$\mathbf{S}'(s)$	scattering matrix of the passive sub-network	[4]
$\mathbf{S}_b(s)$	scattering matrix of the active block b	
$\mathbf{M}_N(s)$	stability matrix in scattering representation $\mathbf{S}'(s)\,\mathbf{S}(s) - \mathbf{1}$	[4]
$\Delta(s)$	characteristic polynomial in scattering representation $\det[\mathbf{M}_N(s)]$	[4]
$\underline{G}_k(s)$	loop gain of the reduced network at step k in Ohtomo's test	[4]
$E[\cdot]$	operator counting with sign the number of clockwise encirclements of the origin made by its argument	

TABLE 2. Definition of main acronyms used throughout the paper.

Acronym	Definition
EDA	Electronic Design Automation
HB	Harmonic Balance
LSSS	Large-Signal/Small-Signal
AG	Auxiliary Generator
HPA	High-Power Amplifier
MIC	Microwave Integrated Circuit
MMIC	Monolithic Microwave Integrated Circuit

When the conversion matrix of a sub-network is required, the outlined procedure assumes that the sub-network under test is appropriately separated from the whole circuit by means of ideal filters: see again [20] for further details.

III. PARTITIONED OHTOMO TEST

Let us recall a fundamental relationship, implicit in [4] and pointed out in [24], between the determinant of the stability matrix $\mathbf{M}_N(s)$ and the loop gains $\underline{G}_k(s)$:

$$\det[\mathbf{M}_N(s)] = \Delta(s) \triangleq \prod_{k=1}^{N} \left(\underline{G}_k(s) - 1\right) \tag{2}$$

Hence, the following observation can be made, which represents the basis for the partitioned Ohtomo test proposed in this contribution. Namely, the multiplicative nature of the expression of $\Delta(s)$ makes it so that the various factors can be grouped arbitrarily:

$$\Delta(s) = \prod_{b=1}^{B} \Delta_b(s) \tag{3}$$

where, for the time being, $\Delta_b(s)$ is simply a sub-product of the form:

$$\Delta_b(s) = \prod_{k \in K_b} \left(\underline{G}_k(s) - 1\right) \tag{4}$$

and K_b are disjoint sets of indexes whose union is $\{k : 1, 2, \ldots, N\}$.

Then, denoting with $E[\cdot]$ an operator counting with sign the number of encirclements of the origin made by its argument (clockwise encirclements corresponding to positive counts) allows to write:

$$E[\Delta] = \sum_{b=1}^{B} E[\Delta_b] \tag{5}$$

A noteworthy possibility is by collecting in separate sub-products all the factors relevant to each active block of

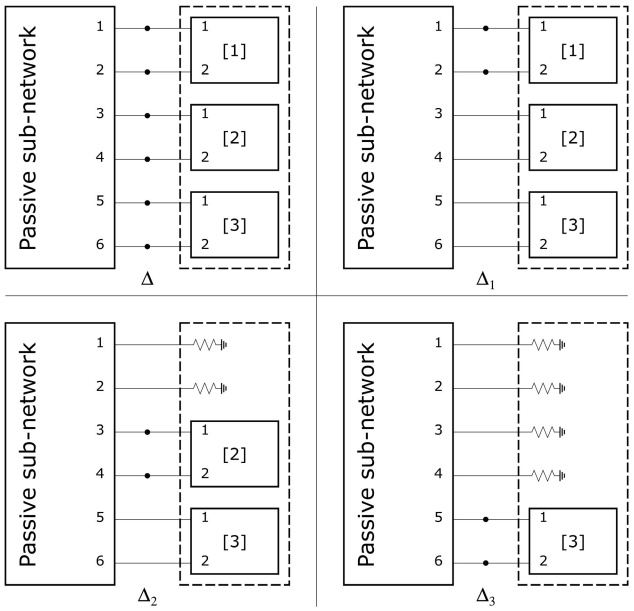

FIGURE 1. Principle of the Ohtomo test splitting exemplified in the case $B = 3$, $n_1 = n_2 = n_3 = 2$. One obtains that $\Delta = \Delta_1 \cdot \Delta_2 \cdot \Delta_3$. The test points are marked by black circles.

the active sub-network, namely:

$$\Delta_b(s) \triangleq \prod_{k=N_b+1}^{N_b+n_b} \left(\underline{G}_k(s) - 1\right) \tag{6}$$

where n_b is the number of terminals of the b-th block and:

$$N_b \triangleq \sum_{l=1}^{b-1} n_l \tag{7}$$

which equals $0, n_1, n_1 + n_2, \ldots, N - n_B$ for b equal to $1, 2, 3, \ldots, B$.

To illustrate, consider the simple case depicted in Fig. 1, i.e., $B = 3$, $n_1 = n_2 = n_3 = 2$. The baseline test corresponds to the upper-left frame, with 6 test points: this would yield the full determinant $\Delta(s)$ as per (2). The other frames depict the test conditions corresponding to (6), with b equal to 1 (upper-right), 2 (lower-left) and 3 (lower-right). The product of the associated sub-factors (Δ_1, Δ_2 and Δ_3, respectively) gives back Δ. Notice that, since the active blocks in Fig. 1 are isolated, the blocks associated with $b < \bar{b}$ are in effect replaced by normalization impedances when solving sub-problem $\bar{b}$.

Notice, from the definition of $\mathbf{M}_N(s)$ and $\underline{G}_k(s)$ in [4], that both the standard and the partitioned Ohtomo test can be applied algebraically directly on the sub-circuit matrices rather than through circuit operations (i.e., rather than by computing reflectances as in [4]).

Finally, notice that the partitioned test reduces to the standard test if one chooses $B = 1$, $n_1 = N$, i.e., if all active devices are grouped together in one single block. Conversely, the minimum granularity resulting in computational advantages is obtained by setting B equal to the number of active devices: indeed, even if it is possible to split a device across multiple blocks, such a choice would nullify the advantages of the proposed partitioning.

IV. EFFICIENCY IMPROVEMENT IN THE NONLINEAR CASE

The discussion in Section III holds true in general for small-signal ($H = 0$) and large-signal ($H > 0$) solutions. However, in the latter case, it is implicit that each physical port corresponds to $2H + 1$ virtual ports at different frequency shifts with respect to the nominal perturbation frequency, consistently with the standard theory of conversion matrices [2]. Thus, $N = (2H + 1)P$ in the large-signal case, which entails a much larger computational burden as compared to the small-signal case. For this reason the partitioned approach is of limited utility if $H = 0$ but is more and more advantageous as H increases.

In the typical situation where all blocks have the same number of physical terminals p_b (with $p_b = 2$ in most cases), the partitioned Ohtomo test would yield matrices of size $[(2H + 1)\,p_b] \times [(2H + 1)\,p_b]$, in a sequence of B sub-tests. As opposed to this, the standard test would involve matrices of size $[(2H + 1)\,p_b B] \times [(2H + 1)\,p_b B]$. Thus, the complexity growth effectively decreases from being quadratic to being linear in B. As a matter of fact, to compare the two approaches, it is worth defining an index of complexity C as the number of elements which need to be computed to fill in the required conversion matrices. From the above we have:

$$C = \begin{cases} (2H+1)^2\, p_b^2 B^2 & \text{standard test} \\ (2H+1)^2\, p_b^2 B & \text{partitioned test} \end{cases} \tag{8}$$

To further improve efficiency, the authors' implementation computes automatically the required conversion matrices starting from a unique sweep of the perturbation frequency, f_{SS}. The sweep is devised in such a manner that, for each nominal perturbation frequency, it contains the other perturbation frequencies at $|f_{SS} + hf_{LS}|$ which are required to fill in the conversion matrix, where $-H \le h \le +H$.

As compared to previous work [20], the present implementation exhibits also other important improvements which it is worthwhile to mention for their impact on the numerical accuracy of the results, simulation time and frequency range. First, it allows for arbitrarily high perturbation frequencies, and that without the introduction of truncation errors for $f_{SS} > 1/2 f_{LS}$. Second, it relies on algebraic manipulations (rather than circuit reconfigurations) to compute the conversion matrices and the loop gains, which makes it more efficient and robust. Notice that the capability of computing automatically the full conversion matrix over frequency of a nonlinear circuit is in itself a remarkable feature, with further applications in mixer design and nonlinear noise analysis.

V. EXPERIMENTAL VALIDATION

A. DUT INTRODUCTION

To illustrate the application of the presented approach to a practical case, the unstable version of a hybrid balanced amplifier discussed in [9] and [25] is selected as an example.

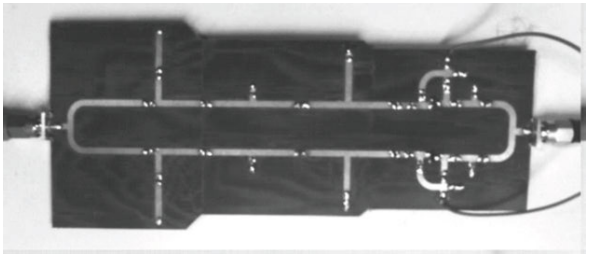

FIGURE 2. Picture of the balanced amplifier.

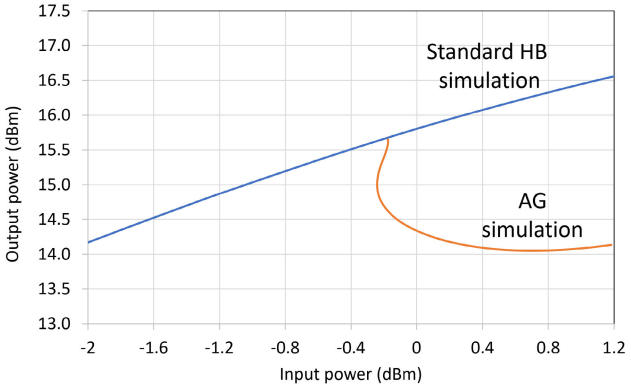

FIGURE 3. Comparison of the simulated output power curves found through standard HB analysis and with the AG technique.

The amplifier is based on BFR92A medium-power silicon bipolar transistors from Infineon in a SOT23 package, which come with a Gummel-Poon nonlinear model including the package parasitics. The amplifier is fabricated on a TLX-8 substrate from Taconic, with surface-mount passive devices characterized by S-parameters from the supplier. In the operative bandwidth of 560 through 580 MHz, the amplifier exhibits a 16.4 dB linear gain with ±0.1 dB ripple, input return loss better than 10 dB, output return loss better than 8 dB and a 19 dBm output power at 1-dB gain compression. As can be seen from Fig. 2, the architecture consists of two identical single-transistor branches in common-emitter configuration, connected by an input splitter and an output combiner.

Since $B = 2$ in this example, the amplifier makes for an ideal case study since $B > 1$ (otherwise, there would be no difference with the standard approach) and at the same time B is low enough that the standard approach is still manageable. In addition, the stability-related behavior of this amplifier is well known thanks to extensive alternative analyses and measurements [9], [25].

In particular, given the nominal operating conditions $V_{CC} = 7.5$ V, $V_{be} = 0.826$ V, the analysis methods used in [9] and [25] reveal that the amplifier is stable at small signal but shows a bifurcation at higher power levels when the frequency of the input signal (f_{LS}) spans from 574 MHz to 588 MHz. Considering, for instance, $f_{LS} = 576$ MHz, at around −0.2 dBm input power a frequency division by 2 occurs and the amplifier generates a subharmonic component at $f_{LS}/2$. The bifurcation is clearly visible in Fig. 3,

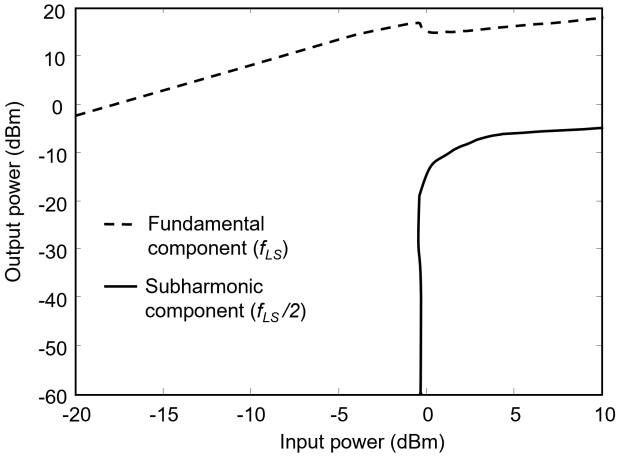

FIGURE 4. Measured output power at fundamental ($f_{LS} = 576$ MHz) and subharmonic frequency ($f_{LS}/2$).

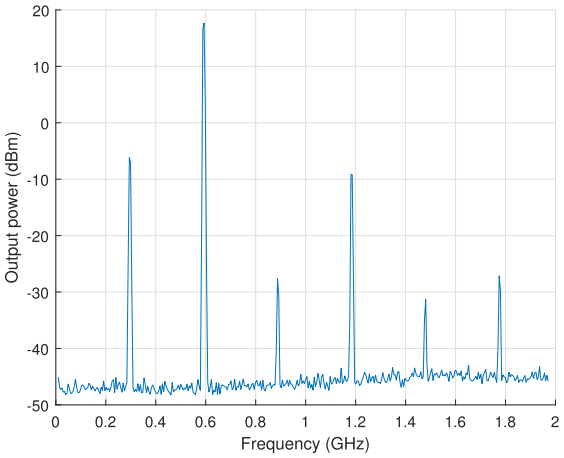

FIGURE 5. Measured output power spectrum at $f_{LS} = 576$ MHz, $P_{av} = 10$ dBm.

where the circuit is analyzed through the auxiliary-generator (AG) technique, for which the reader is referred to [3].

The parametric instability of the amplifier was verified through measurements. In particular, Fig. 4 reports the measured results of a sweep of the available input power (P_{av}) at nominal frequency $f_{LS} = 576$ MHz. The output power at the fundamental frequency increases continuously until the bifurcation is reached, then the subharmonic component kicks in at frequency $f_{LS}/2$. These experimental results agree very well with the simulations in Fig. 3. Further, Fig. 5 shows an example of the measured output spectrum after the bifurcation. The division-by-2 of the frequency basis is clearly visible.

B. PROPOSED TEST

The amplifier was then subjected to the stability analysis approach presented in this contribution. A LSSS simulation with $H = 5$ was set up at nominal conditions and at different values of P_{av}, with a 1-dB step. The partial determinants Δ_1 and Δ_2 were found to trace Nyquist plots void of encirclements of the critical point (i.e., the origin in this

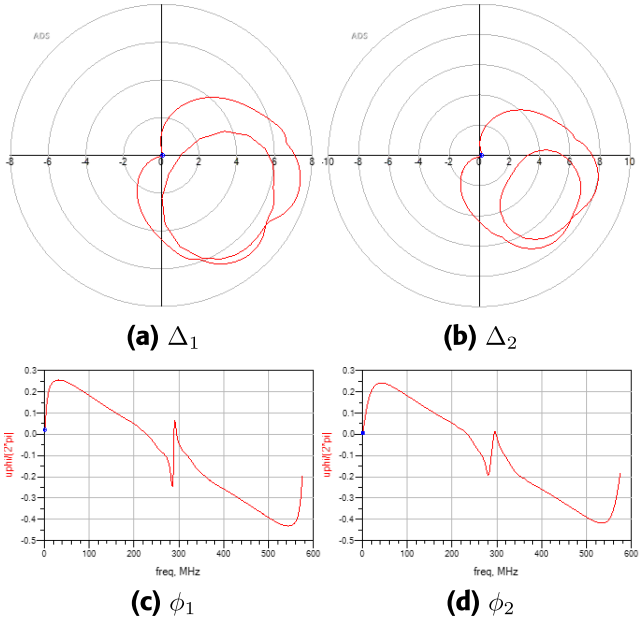

FIGURE 6. $_i$ and $\phi_i = \angle\Delta_i$ of the balanced amplifier, computed either through the standard or partitioned method. Simulation parameters: $P_{av} = -1$ dBm, $f_{LS} = 576$ MHz, $H = 5$.

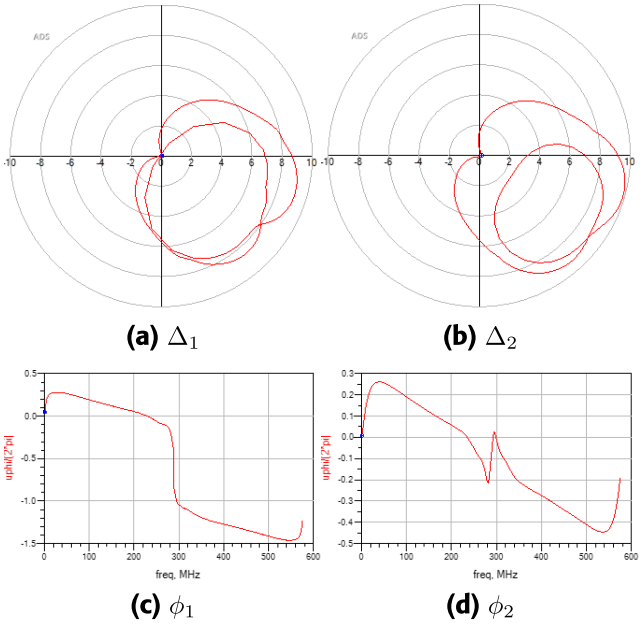

FIGURE 7. Δ_i and $\phi_i = \angle\Delta_i$ of the balanced amplifier, computed either through the standard or partitioned method. Simulation parameters: $P_{av} = 0$ dBm, $f_{LS} = 576$ MHz, $H = 5$.

representation) for P_{av} up to -1 dBm, i.e., $E[\Delta] = E[\Delta_1] + E[\Delta_2] = 0$. In particular, the partial determinants and their phases are shown in Fig. 6.

The above results indicate that, subject to the inherent-stability proviso (see Section V-D), $\Delta(s)$ does not exhibit unstable zeros for $P_{av} \leq 0$ dBm, whereas conjugate pairs of unstable zeros appear at higher driving levels – each pair being relevant to the $[0, f_{LS}]$ range and to the subsequent f_{LS}-wide bands. As emerges from Fig. 7-(a) and (c), the Nyquist plot of Δ_1 runs very close to the critical point at a frequency $f_{cr} = f_{LS}/2$, which denotes a zero with imaginary part $\omega_{cr} = 2\pi f_{cr} = \pi f_{LS}$: a rather typical behavior.

Thus, the proposed approach agrees very well both with alternative simulations approaches and with measurements, either illustrated in this contribution (Figs. 3-5) or presented elsewhere [9], [25]. In addition, the loop gains computed with the proposed method and shown in Figs. 8-9 are *numerically identical* to those computed through the standard method [20], which further validates the presented partitioning approach. As compared to the latter method, however, it entails significantly shorter processing times, due to the reasons discussed in Section IV. This will be shown quantitatively in Section V-C and in particular in Table 3.

C. EFFICIENCY COMPARISON

In order to provide a quantitative comparison, in terms of simulation efficiency, between the standard and the partitioned approach, the considered balanced amplifier was subjected to both on the same machine, namely, a computer equipped with an Intel(R) Core(TM) i5-1035G1 4-core processor, an x64 operating system and 16 GB RAM. The standard and partitioned tests lead to a processing time of the data set as reported in Table 3. In order to obtain reasonable processing times, the frequency sweep was kept unusually low, namely 50 points between d.c. and the fundamental frequency of the large-signal excitation, f_{LS}. The values in parentheses are quadratic extrapolations of the $B = 1$ case (in this example, $B \leq 2$). However, it is worth noticing that for the verified condition at $B = 2$ the actual processing time with the standard approach was found to be even higher (13.15 s or 45.72 s) than the theoretically expected one (10.80 s or 29.40 s). For more complex circuits (larger B or p_b) or more demanding simulation conditions (larger H or F, where F is the number of small-signal frequency points), the partitioned approach would obviously become even more advantageous than in this example. Notice also that $p_b = 2$ in this illustration: this corresponds to analyzing B replicas of half the circuit when $B \neq 2$, the actual circuit for $B = 2$.

TABLE 3. Comparison of Processing Time [s] between Standard and Partitioned Ohtomo Test in an Illustrative Case.

B	$H = 3$		$H = 5$	
	standard	partitioned	standard	partitioned
1	2.70	2.70	7.35	7.35
2	13.15 (10.80)	5.40	45.72 (29.40)	14.70
3	(24.30)	8.10	(66.15)	22.05
4	(43.20)	10.80	(117.60)	29.40
10	(270.00)	27.00	(735.00)	73.50

In addition to the processing time, it is worth presenting, in Table 4, the index of complexity C defined in (8), since this is a machine-independent figure of merit. Again, the convenience of the partitioned approach is more and more apparent as B increases and, for $B > 1$, as H increases. Of course, this comparison holds at each small-signal

TABLE 4. Comparison of Index of Complexity C between Standard and Partitioned Ohtomo Test in an Illustrative Case.

B	$H=3$		$H=5$	
	standard	partitioned	standard	partitioned
1	196	196	484	484
2	784	392	1936	968
3	1764	588	4356	1452
4	3136	784	7744	1936
10	19600	1960	48400	4840
$\hat{B}$	$7^2{\cdot}2^2 \cdot \hat{B}^2$	$7^2{\cdot}2^2 \cdot \hat{B}$	$11^2{\cdot}2^2 \cdot \hat{B}^2$	$11^2{\cdot}2^2 \cdot \hat{B}$

frequency, hence the comparative benefits of using the partitioned approach increase as F increases.

D. CHECK OF THE INHERENT-STABILITY PROVISO

As mentioned in Section II, Nyquist-based tests require that some precondition be valid in order to be meaningfully applied. In the case of Ohtomo's test, this is typically referred to as the 'inherent-stability proviso' and requires that the active sub-network be devoid of unstable poles when terminated in reference loads [4], [20]. For completeness, we report on the proviso check in the following.

As usual [18], [20], this was carried out through identification of the scattering conversion matrices of the active blocks [13], [14], [15] at each simulation condition (actually, the conditions for which $E[\Delta] = 0$ would clearly be enough). In this case, since the two active devices operate in identical conditions, it follows that $\mathbf{S}_1(s) = \mathbf{S}_2(s)$, therefore just one identification per simulation condition was sufficient. Also, the full information stored in the computed conversion matrices was used (i.e., instead of cropping the iso-frequency response only) by exploiting the commonality of the poles among all elements [14]. The identification step was carried out in MATLAB through the package VFIT3 [26], [27].

The pole plots resulting for the two driving levels $P_{av} = -1$ dBm and $P_{av} = 0$ dBm are shown in Fig. 8 and Fig. 9, respectively. In both conditions the inherent stability proviso is fulfilled: after all, this is not difficult to achieve, since the active block matrices include isolated devices whose stability is to be evaluated in relation to purely resistive loads of arbitrary value.

E. INSTABILITY CORRECTION

As mentioned in the Introduction, all analysis tools for inherent-stability analysis are based on the idea of localizing the zeros of the characteristic polynomial, and in particular with respect to the vertical axis of the complex plane. This is done directly in the case of the identification-based techniques, and indirectly (i.e., by studying the stability margins) in the case of the Nyquist-based techniques. In either case, however, since the zeros of the characteristic polynomial are a global property of the network, no clear indications are provided to the designers as to how and where modify an unstable circuit to cure the instability.

This limitation is circumvented in practice by iterating the analysis over sweeps of circuit parameters which are likely to impact its stability properties. In turn, the choice of these parameters is based on common sense and design experience. In particular, a common cause of oscillation in corporate amplifiers consists in the emergence of odd-mode instabilities related to the presence of loops across symmetry planes. These instabilities are typically corrected by adding appropriate resistors across those symmetry planes, thus damping the odd modes [14], [15], [25].

As a matter of fact, this very strategy has been proven successful in the case of the balanced amplifier here considered. Specifically, it has been shown in [25] that inserting a resistor of 47 Ω between the two points just ahead of the gate d.c.-block capacitors manages to stabilize the circuit.

The same analysis is repeated here by means of the proposed approach, to show that consistent results are again obtained with alternative analysis approaches and measurements. Fig. 10 juxtaposes the Nyquist and phase plot of $\Delta_1(s)$ for the unstable (left) and stabilized (right) circuit versions. As already observed in Section V-B, $\Delta_1(s)$ of the unstable circuit exhibits an encirclement of the origin at the critical frequency $f_{cr} = f_{LS}/2$. After adding the stabilization resistance, however, the encirclement of the origin vanishes as expected.

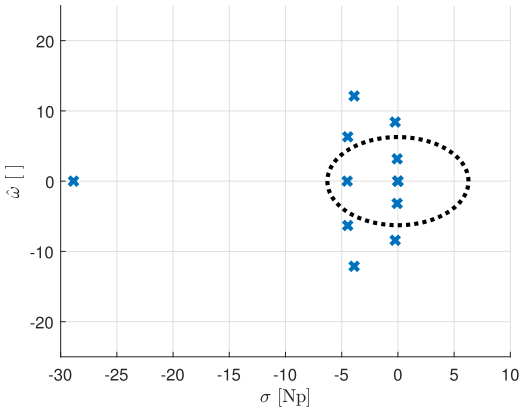

FIGURE 8. Identified poles of $\mathbf{S}_i(s)$ of the balanced amplifier at nominal condition for $P_{av} = -1$ dBm. The angular frequency is normalized to that of the large-signal tone and the dashed curve represents the circumference $|\sigma + j\hat{\omega}| = \hat{\omega}_{max}$. All poles are in the left-hand half plane.

VI. APPLICATION TO A COMPLEX MMIC

Since the proposed method is aimed at realistic circuits with a large number of active devices, another example is presented in this Section, constituted by a complex MMIC realized on MACOM's GaN-on-Si technology. The MMIC implements a distributed high-power amplifier (HPA) with 5-50 GHz bandwidth and comprising eight cascode pairs, for a total of 16 active devices. In order to improve the gain while guaranteeing good output power, the common-source and common-gate stages of the cascode pairs are featured by 60-nm and 100-nm gate lengths, respectively. The simultaneous use, on the same circuit, of two different gate lengths is a peculiarity of the adopted technology.

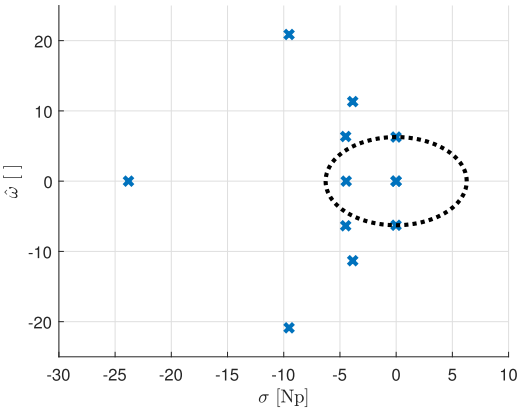

FIGURE 9. Identified poles of $S_i(s)$ of the balanced amplifier at nominal condition for $P_{av} = 0$ dBm. The angular frequency is normalized to that of the large-signal tone and the dashed curve represents the circumference $|\sigma + j\hat{\omega}| = \hat{\omega}_{max}$. All poles are in the left-hand half plane.

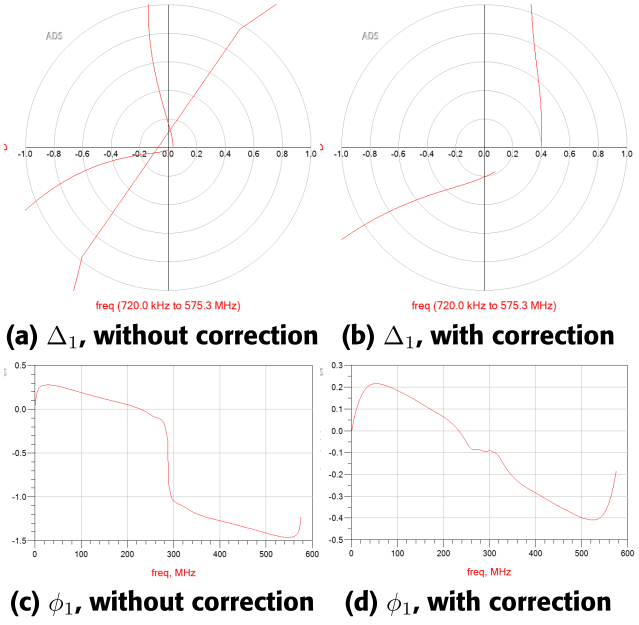

FIGURE 10. Δ_1 and $\phi_1 = \angle\Delta_1$ of the balanced amplifier, computed either through the standard or partitioned method. Simulation parameters: $P_{av} = 0$ dBm, $f_{LS} = 576$ MHz, $H = 5$. Left: without stabilization resistance. Right: with stabilization resistance.

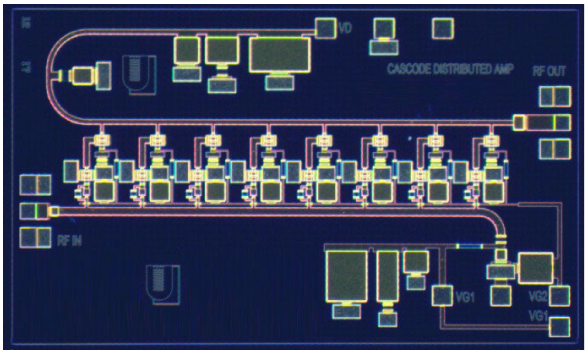

FIGURE 11. Picture of the distributed HPA.

The details of the HPA, which is shown in Fig. 11, will be presented in a future publication. However, it is here mentioned that measured performance includes input and output return losses better than 10 dB over the whole operative bandwidth, as well as a gain of approximately 10 dB. The measured output power at 1 dB gain compression

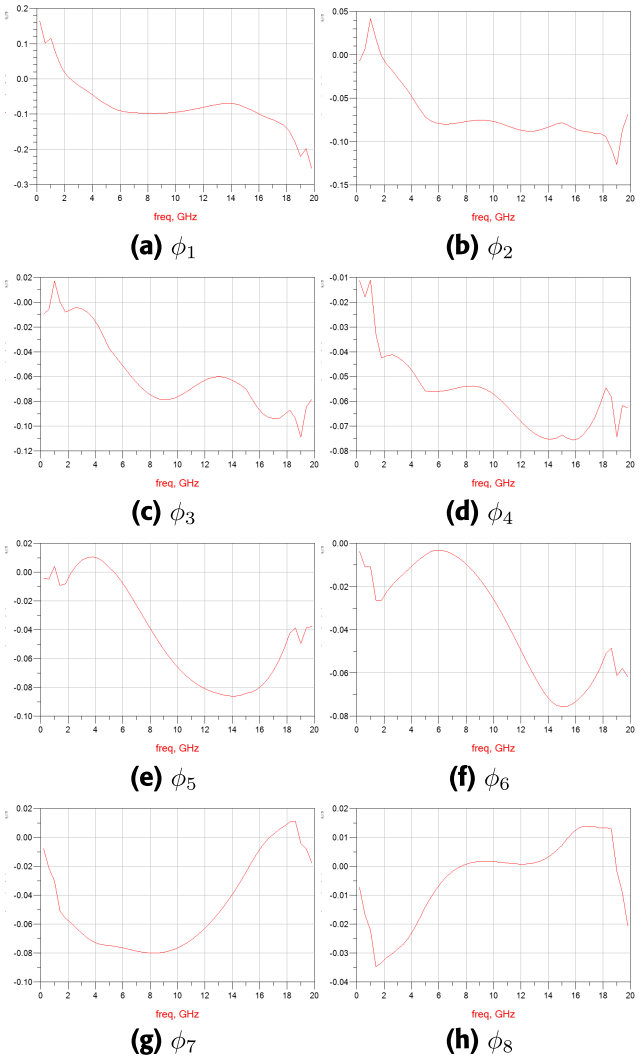

FIGURE 12. $\phi_i = \angle\Delta_i$ of the distributed HPA, computed either through the standard or partitioned method. Simulation parameters: $P_{av} = 23$ dBm, $f_{LS} = 20$ GHz, $H = 2$.

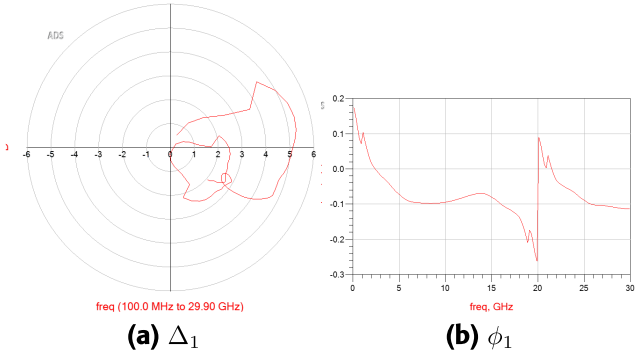

FIGURE 13. Detail of Δ_1 and $\phi_1 = \angle\Delta_1$ of the distributed HPA, computed either through the standard or partitioned method. Simulation parameters: $P_{av} = 23$ dBm, $f_{LS} = 20$ GHz, $H = 2$.

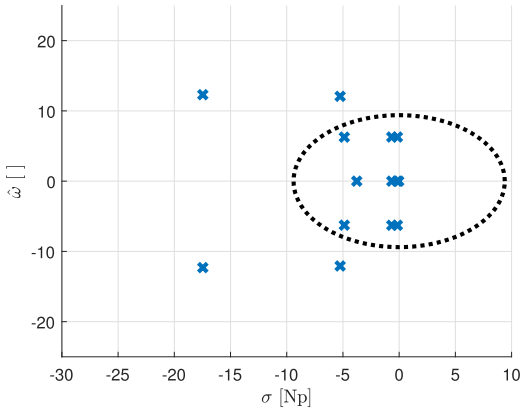

FIGURE 14. Identified poles of $S_i(s)$ of the distributed HPA at nominal condition for $P_{av} = 23$ dBm. The angular frequency is normalized to that of the large-signal tone and the dashed curve represents the circumference $|\sigma + \jmath\hat{\omega}| = \hat{\omega}_{max}$. All poles are in the left-hand half plane.

is about 25 dBm for frequencies between 5 GHz and 25 GHz, although it decreases more or less linearly to 16 dBm between 25 GHz and 50 GHz. Chip size is 3.0×1.8 mm^2.

Given the large number of active devices, the problem was simplified upfront by including in the active blocks the whole cascode pairs rather than the individual devices. The latter approach would have entailed two ports for each common-source device and three ports for each common-gate device, for a total of 40 ports for both the passive and active sub-networks; in addition, the N_b values would have been different for the common-source and common-gate devices (2 and 3, respectively), complicating further the overall setup. The adopted simplification, on the other hand, reduces the ports of the two sub-networks to 16 – still a rather challenging number, and totally out of reach for the standard method.

Fig. 12 shows the result of the analysis, with the HPA operating at nominal conditions and driven by a 23-dBm continuous wave at 20 GHz. The perturbation frequency is swept up to f_{LS} in 50 uniformly spaced steps. Although no encirclements of the critical point are found, the small jump of ϕ_1 around f_{LS} was deemed to deserve further investigation. Thus, a new analysis, limited to the first block but up to higher frequency ($^3/_2 f_{LS}$) and with a finer step (150 points in total) was carried out. It is worth noting that, with the standard approach, it would not have been possible to selectively refine the analysis parameters as here shown. The detailed analysis of the first block is shown in Fig. 13. It can be seen that the jump is actually not associated with an encirclement but simply with a crossing of the real axis to the right of the origin.

Finally, the inherent-stability proviso was checked on the active blocks. Again, since these are identical and exhibit the same operating point, only one block per driving level needs to be checked. The pole plot associated with the data in Fig. 13 is shown in Fig. 14. The identification method is the same as already illustrated in Section V-D.

VII. CONCLUSION

This contribution has shown that the structure of the active sub-network (in particular, the mutual isolation of the active components) arising in the Ohtomo test can be exploited to split the computation into a sequence of smaller tests. These remarks apply equally well to d.c. and large-signal solutions; however, they allow a notably more efficient implementation of the Ohtomo test in the large-signal case. The strong points of the current implementation, as compared to former ones, have been discussed. The proposed large-signal Ohtomo test has been validated against a hybrid balanced amplifier, whose stability behavior is well known from previous work. In addition, it has been applied to a realistic MMIC with a large number of devices, i.e., such that the standard method is on the contrary not feasible.

REFERENCES

[1] V. Rizzoli and A. Neri, "State of the art and present trends in nonlinear microwave CAD techniques," *IEEE Trans. Microw. Theory Techn.*, vol. 36, no. 2, pp. 343–365, Feb. 1988.

[2] S. A. Maas, *Nonlinear Microwave and RF Circuits*, 2nd ed. Norwood, MA, USA: Artech House, 1997.

[3] A. Suárez and R. Quéré, *Stability Analysis of Nonlinear Microwave Circuits*. Norwood, MA, USA: Artech House, 2003.

[4] M. Ohtomo, "Stability analysis and numerical simulation of multidevice amplifiers," *IEEE Trans. Microw. Theory Techn.*, vol. 41, no. 6, pp. 983–991, Jun./Jul. 1993.

[5] A. Platzker and W. Struble, "Rigorous determination of the stability of linear N-node circuits from network determinants and the appropriate role of the stability factor K of their reduced two-ports," in *Proc. 3rd Int. Workshop Integr. Nonlinear Microw. Millimeterwave Circuits*, Jan. 1994, pp. 93–107.

[6] M. L. Edwards and J. H. Sinsky, "A new criterion for linear 2-port stability using a single geometrically derived parameter," *IEEE Trans. Microw. Theory Techn.*, vol. 40, no. 12, pp. 2303–2311, Dec. 1992.

[7] J. Rollett, "Stability and power-gain invariants of linear twoports," *IRE Trans. Circuit Theory*, vol. 9, no. 1, pp. 29–32, 1962.

[8] H. W. Bode, *Network Analysis and Feedback Amplifier Design*. New York, NY, USA: Van Nostrand, 1945.

[9] A. Santarelli, L. Pantoli, G. Leuzzi, and F. Filicori, "Stability characterizing function for electronic circuit design based on frequency-domain analysis with parametric damping," *IEEE Trans. Microw. Theory Techn.*, vol. 72, no. 3, pp. 1536–1550, Mar. 2024.

[10] S. Hernández and A. Suárez, "Systematic methodology for the global stability analysis of nonlinear circuits," *IEEE Trans. Microw. Theory Techn.*, vol. 67, no. 1, pp. 3–15, Jan. 2019.

[11] A. Cooman, F. Seyfert, M. Olivi, S. Chevillard, and L. Baratchart, "Model-free closed-loop stability analysis: A linear functional approach," *IEEE Trans. Microw. Theory Techn.*, vol. 66, no. 1, pp. 73–80, Jan. 2018.

[12] L. Pantoli, "Transient-based conversion matrix approach for nonlinear stability analysis," *Electron. Lett.*, vol. 50, no. 13, pp. 923–925, Jun. 2014.

[13] A. Anakabe, N. Ayllón, J. M. Collantes, A. Mallet, G. Soubercaze-Pun, and K. Narendra, "Automatic pole-zero identification for multivariable large-signal stability analysis of RF and microwave circuits," in *Proc. 40th Eur. Microw. Conf.*, Sep. 2010, pp. 477–480.

[14] L. Mori, A. Anakabe, I. Lizarraga, N. Otegi, J.-M. Collantes, V. Armengaud, and G. Soubercaze-Pun, "Stability analysis of multistage power amplifiers using multiple-input multiple-output identification," in *IEEE MTT-S Int. Microw. Symp. Dig.*, May 2016, pp. 1–4.

[15] L. Mori, I. Lizarraga, A. Anakabe, J.-M. Collantes, V. Armengaud, and G. Soubercaze-Pun, "Efficient calculation of stabilization parameters in RF power amplifiers," *IEEE Trans. Microw. Theory Techn.*, vol. 68, no. 9, pp. 3686–3696, Sep. 2020.

[16] S. Mons, J.-C. Nallatamby, R. Quere, P. Savary, and J. Obregon, "A unified approach for the linear and nonlinear stability analysis of microwave circuits using commercially available tools," *IEEE Trans. Microw. Theory Techn.*, vol. 47, no. 12, pp. 2403–2409, Dec. 1999.

[17] V. Rizzoli and A. Lipparini, "General stability analysis of periodic steady-state regimes in nonlinear microwave circuits," *IEEE Trans. Microw. Theory Techn.*, vol. MTT-33, no. 1, pp. 30–37, Jan. 1985.
[18] A. Suárez and F. Ramírez, "Two-level stability analysis of complex circuits," *IEEE Trans. Microw. Theory Techn.*, vol. 69, no. 1, pp. 132–146, Jan. 2021.
[19] F. L. Traversa, F. Bonani, and S. D. Guerrieri, "A frequency-domain approach to the analysis of stability and bifurcations in nonlinear systems described by differential-algebraic equations," *Int. J. Circuit Theory Appl.*, vol. 36, no. 4, pp. 421–439, Jun. 2008.
[20] S. Colangeli, W. Ciccognani, P. E. Longhi, L. Pantoli, G. Leuzzi, and E. Limiti, "Extending the Ohtomo stability test to large-signal solutions in a commercial circuit simulator," *IEEE Trans. Microw. Theory Techn.*, vol. 69, no. 10, pp. 4437–4447, Oct. 2021.
[21] Official Website. *Keysight*. Accessed: Jun. 1, 2023. [Online]. Available: https://www.keysight.com/it/en/products/software/pathwave-design-software/pathwave-advanced-design-system.html
[22] OfficialWebsite. *Cadence*. Accessed: Mar. 21, 2024. [Online]. Available: https://www.cadence.com/en_US/home/tools/system-analysis/rf-microwave-design/awr-microwave-office.html
[23] Official Website. *MathWorks*. Accessed: Mar. 21, 2024. [Online]. Available: https://it.mathworks.com/products/MATLAB.html
[24] S. Colangeli, R. Cleriti, D. Palombini, and E. Limiti, "On the unconditional stability of N-port networks," in *Proc. 44th Eur. Microw. Conf.*, Oct. 2014, pp. 1520–1523.
[25] L. Pantoli, G. Leuzzi, A. Santarelli, and F. Filicori, "Stability analysis and design criteria of paralleled-device power amplifiers under large-signal regime," *IEEE Trans. Microw. Theory Techn.*, vol. 64, no. 5, pp. 1442–1455, May 2016.
[26] B. Gustavsen, "Improving the pole relocating properties of vector fitting," *IEEE Trans. Power Del.*, vol. 21, no. 3, pp. 1587–1592, Jul. 2006.
[27] B. Gustavsen and A. Semlyen, "Rational approximation of frequency domain responses by vector fitting," *IEEE Trans. Power Del.*, vol. 14, no. 3, pp. 1052–1061, Jul. 1999.

SERGIO COLANGELI was born in Rome, Italy, in 1984. He received the Ph.D. degree in telecommunications and microelectronics from the University of Rome Tor Vergata, Rome, in 2013. He has been with the Electronics Department, University of Rome Tor Vergata, where he is currently an Associate Professor. His research interests include low-noise design methodologies for microwave applications, with particular reference to low-noise amplification, small-signal and noise characterization, modeling of microwave active devices, and stability analysis of linear and nonlinear circuits. He was a recipient of the EuMIC Young Engineer Prize, in 2012.

LEONARDO PANTOLI (Member, IEEE) received the degree (cum laude) in electronic engineering and the Ph.D. in electrical and information engineering from the University of L'Aquila, Italy, in 2006 and 2010, respectively. From 2007 to 2008, he spent several months with DICOM, University of Cantabria, Spain, and the C2S2 Department, XLIM Research Institute, France. Currently, he is an Associate Professor with the University of L'Aquila and he is qualified to function as a Full Professor. His research activities include the development of methods and algorithms for the design of RF, microwave, and millimeter wave nonlinear circuits; stability analysis of circuits in both linear and large-signal regime; active filters design; and MMICs design for aerospace wireless communication and imaging application.

WALTER CICCOGNANI was born in Rome, Italy, in 1977. He received the M.S. degree in electronic engineering and the Ph.D. degree in telecommunications and microelectronics from the University of Rome Tor Vergata, Rome, in 2002 and 2007, respectively. Since 2012, he has been an Assistant Professor with the University of Rome Tor Vergata, where he has been teaching the course in microwave measurements, since 2013. He has coauthored over 60 papers in international scientific journals and conferences. He has been involved in several national and international research projects, and in those contexts he has the opportunity to collaborate with the major European semiconductor foundries. His main interests include linear microwave circuit-design methodologies, linear and noise analysis/measurement techniques, and small-signal and noise modeling of microwave active devices.

PATRICK E. LONGHI (Member, IEEE) received the M.S. degree in electronic engineering and the Ph.D. degree in microelectronics from the University of Rome Tor Vergata, Italy, in 2004 and 2009, respectively. From 2009 to 2018, he was with ELT-Elettronica SpA, Rome, Italy, holding different managerial and technical positions in engineering, manufacturing, and sales. Since August 2018, he has been an Assistant Professor with the Electronic Engineering Department, University of Rome Tor Vergata. His main fields of interests include the design of microwave and millimeter-wave LNAs and RF amplitude control circuits (variable gain amplifiers and attenuators) and mixers.

GIORGIO LEUZZI received the degree (cum laude) in electronic engineering from the University of Rome La Sapienza, Italy, in 1982. In 1984, he became a Teaching and Research Assistant with the University of Rome Tor Vergata, Italy, where he has been teaching microwave electronics, since 1991. In 1998, he became an Associate Professor and in 2001 a Full Professor of electronic devices with the University of L'Aquila, Italy. His research activities include the simulation of semiconductor devices for microwaves and millimeter waves, the linear and nonlinear characterization of microwave and millimeter-wave active devices, the development of methods and algorithms for microwave nonlinear circuit design, and the design of microwave active filters.

ERNESTO LIMITI (Senior Member, IEEE) was a Research and Teaching Assistant (1991–1997), an Associate Professor (1998–2001), and has been a Full Professor (since then) of electronics with the EE Department, University of Rome Tor Vergata, Rome, Italy. He has been the President of the Laurea and Laurea Magistrale degrees in electronic engineering with the University of Rome Tor Vergata. He is a member of the committee of the Ph.D. program in telecommunications and microelectronics and tutoring an average of four doctoral candidates per year. He has authored or coauthored over 350 publications on refereed international journals and presentations within international conferences. His research activity is focused on three main lines, all of them belonging to the microwave and millimeter-wave electronics area. The first one is related to characterization and modeling for active and passive microwave and millimeter-wave devices. Regarding active devices, the research line is oriented to small-signal, noise, and large-signal modeling. For active devices, novel methodologies have been developed for the noise characterization and the subsequent modeling, and equivalent-circuit modeling strategies have been implemented both for small- and large-signal operating regimes for GaAs, GaN, SiC, Si, and amd InP MESFET/HEMT devices. The second line is related to design methodologies and characterization methods for low-noise devices and circuits. The main focus is on cryogenic amplifiers and devices. Finally, the third line is in the analysis and design methodologies for linear and nonlinear microwave circuits. He is a referee for international journals of the microwave and millimeter-wave electronics sector. He is a member of the steering committee of international conferences and workshops.

Open Access funding provided by 'Università degli Studi di Roma "Tor Vergata"' within the CRUI CARE Agreement